ACS OMEGA

Open Access

http://pubs.acs.org/journal/acsodf

Article

Uncovering the Aggregation-Induced Emission Mechanisms of Phenoxazine and Phenothiazine Groups

Yan-Ping Lin, Ying Gao,* Yong Wu, and Xiao-Dong Yang*

Cite This: *ACS Omega* 2024, 9, 26112−26120

Read Online

ACCESS | Metrics & More | Article Recommendations | Supporting Information

ABSTRACT: Molecules with both aggregation-induced emission (AIE) and thermally activated delayed fluorescence (TADF) properties are potential organic light-emitting diode materials; however, the AIE and TADF mechanisms are still debatable. In this work, four molecules incorporating carbazole (**Cz**), phenoxazine (**PXZ**), and phenothiazine (**PTZ**) as donor groups to the diphenylsulfone acceptor were investigated. The experiment results indicate that a molecule containing **Cz** exhibits solely TADF properties, whereas molecules containing **PXZ** and **PTZ** demonstrate both TADF and AIE characteristics. As for **DPS-PTZ**, the result indicates that the thin-film environment restricts molecular twisting, consequently reducing nonradiative decay, thereby attributing to the AIE property by density functional theory and molecular dynamics simulation. As for **DPS-PXZ**, the result suggests that the restricted access to a conical intersection in a singlet excited via an expansion in the C−S−C angle is the pivotal factor for the AIE characteristic. The C−S−C angle twist of **DPS-PXZ** is impeded in the aggregate state and resulted in luminescence. Understanding the mechanisms serves as a valuable guide for the development of new AIE systems, enabling their application in various practical domains.

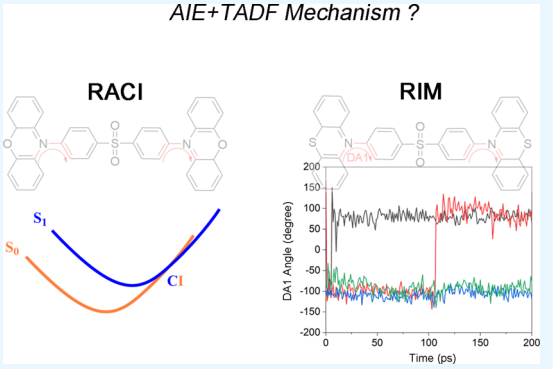

1. INTRODUCTION

The organic light-emitting diode (OLED) technologies have presented a continual challenge for chemists ever since Tang and Van Slyke's pioneering report on OLED in 1987.[1] Examining the history of OLED materials, the purely organic materials with delayed fluorescence possess theoretically a 100% internal quantum efficiency due to their small singlet−triplet energy splitting (ΔE_{ST}) and efficient conversion of triplet excitons (75%) into singlet excitons.[2−5] However, achieving high efficiency remains a complex issue due to the occurrence of aggregation-caused quenching (ACQ) effects when considering the application of OLED applications. ACQ effect typically arises when luminophore is utilized in the aggregate state as thin solid films.[6,7]

In 2001, Tang and colleagues observed a substantial increase in fluorescence upon adding water to a solution of 1-methyl-1,2,3,4,5-pentaphenylsilole in ethanol, a phenomenon termed aggregation-induced emission (AIE). Unlike conventional chromophores, luminogens exhibiting AIE effectively overcome ACQ issues, where their emissions are augmented by aggregation.[8] Subsequently, the Tang group played a pivotal role in significantly advancing the application of AIE phenomena, as evidenced by a substantial body of reviews.[9−12] Since the inception of the AIE concept, numerous hypotheses have been proposed to elucidate AIE mechanisms.[13] These include the restriction of intramolecular motion,[14−18] restricted access to a conical intersection,[19] excimer formation, J-aggregates,[20] twisted intramolecular charge transfer (ICT) states,[21,22] and excited-state intramolecular proton transfer.[23] Thanks to the concerted efforts of scientists worldwide, numerous AIEgens based on the restriction of intramolecular motion mechanisms have been developed. These include tetraphenylethene, tetraphenylpyrazine,[24] silole,[25] quinoline-malononitrile,[26] cyanostilbene,[27] 9,10-distrylanthracene,[28] and organoboron complexes.[29]

Experimental evidence has consistently demonstrated that the active intramolecular motion observed in solution becomes restricted upon aggregation or in the solid state. Various methods in experiments have been employed to restrict molecular motions, including incorporating chromophores into high-viscosity media, reducing temperature, doping them within rigid polymer matrices, or embedding them into metal−organic frameworks.[30−34] These molecules typically feature both electron donor and acceptor units, indicating a strong influence of solvent polarity on the properties of the electronic states. Time-resolved fluorescence spectra indicate

Received: February 18, 2024
Revised: May 12, 2024
Accepted: May 27, 2024
Published: June 6, 2024

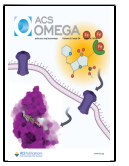

that the efficient occurrence of AIE arises from the elimination of ICT states due to the gradual transition from the local excited state to the ICT with increasing solvent polarity. Consequently, the AIE mechanism stems from the restriction of molecular torsional motion and the hindered transition from the local excited state to the ICT state.[35] Additionally, the AIE mechanism involves the inhibition of nonradiative pathways, specifically the vibrational/torsional energy relaxation process that is impeded in the aggregate state. Studies focusing on boron dipyrromethene derivatives suggest a restricted twisted ICT process.[36]

The molecular engineering aimed at imparting both thermally activated delayed fluorescence (TADF) and AIE characteristics holds promise in realizing efficient nondoped OLEDs with reduced efficiency roll-off and simplified fabrication processes.[37] AIE emission materials exhibit exceptional solid-state emission by mitigating concentration quenching and exciton annihilation, while TADF materials efficiently utilize both electrogenerated single and triplet excitons. Consequently, the collaboration of AIE and TADF presents a rational approach to designing novel, robust luminescent materials. The coexistence of the AIE and TADF phenomena represents a surprising experimental discovery. Despite the recognition of the restriction of intramolecular motion as the general working mechanism for AIE,[38] the underlying mechanisms of some AIE systems remain unclear. Both theoreticians and experimentalists have dedicated efforts to unraveling the AIE mechanism through various works.

Until now, numerous research groups have documented successful instances of combining notable TADF and AIE properties.[39−45] To gain a deep understanding of the working mechanism of AIE-TADF, it is essential to comprehend the structural disparities between typical AIE-TADF and TADF compounds. Utilizing density functional theory methods, a series of structurally identical luminogens (Figure 1) featuring

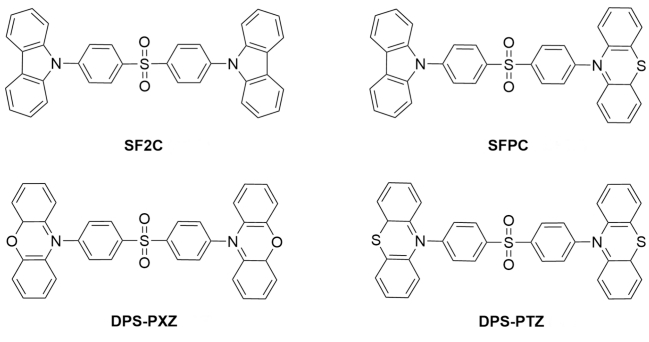

Figure 1. Molecular structures of **SF2C**, **SFPC**, **DPS-PXZ**, and **DPS-PTZ**.

a donor−acceptor framework have been studied. In particular, four molecules containing carbazole (**Cz**), phenoxazine (**PXZ**), and phenothiazine (**PTZ**) as donor groups to diphenylsulfone acceptor have been previously reported.[37] Notably, the experimental results revealed that even a single change in the donor unit results in a dramatic difference in properties: certain molecules exhibit both TADF and AIE properties, while others solely possess TADF characteristics. Subsequently, a comprehensive assessment of various properties was computed to discern the distinctions among these molecules.

2. RESULTS AND DISCUSSION

Actually, two **DPS-PTZ** conformations (quasi-axial and quasi-equatorial) have been demonstrated in experiments, and these different conformations also affect the AIE property. The work by Aydemir et al. suggests that the AIE behavior of **DPS-PTZ** might be a result of solvatochromism demonstrated by various experimental methods.[45] Initially, we optimized both conformations and investigated their electronic properties, as depicted in Figure S1. The energy difference between them is small, at 8 kJ/mol, suggesting that these two conformations (quasi-axial and quasi-equatorial) could coexist under experimental conditions. As illustrated in Figure S1, the two **DPS-PTZ** conformations exhibit notably different HOMO and LUMO distributions. Regarding the HOMO to LUMO transition, **DPS-PTZ** with the quasi-axial conformation shows a local excited state and little solvent stabilization, while **DPS-PTZ** with the quasi-equatorial conformation displays a charge transfer state and undergoes far greater solvent stabilization in polar media. Based on experimental and theoretical results, we speculate that the emission shift may originate from **DPS-PTZ** with a quasi-equatorial conformation. Furthermore, the AIE behavior is attributed to the reduction of nonradiative decay rate, possibly from **DPS-PTZ** with quasi-axial conformation, or both conformations in a thin film environment. Consequently, we further investigate the AIE mechanism originating from **PXZ** and **PTZ** groups by choosing **DPS-PTZ** with a quasi-axial conformation.

For a comprehensive understanding of the solvent effect on the electronic structures of **SF2C**, **SFPC**, **DPS-PXZ**, and **DPS-PTZ**, geometric optimizations were conducted using the density functional theory (DFT) method in toluene (TOL), tetrahydrofuran (THF), and dimethyl sulfoxide (DMSO) solvents. In the ground state (S_0), **Cz** and **PXZ** components adopt planar and rigid conformations. Conversely, the **PTZ** moiety exists in a bonding structure due to a sulfur bridge linking two phenyl rings, resulting in the formation of a nonplanar "butterfly like" structure with a C−C−S−N dihedral angle of approximately 35°. Subsequently, HOMO and LUMO energy levels in TOL, THF, and DMSO solvents were computed based on the optimized S_0 structures (in Figure 2a). The influence of the solvent type exhibited a subtle effect on the HOMO and LUMO energy levels of **SFPC** and **SF2C**. However, for **DPS-PXZ** and **DPS-PTZ**, there were observable variations; the LUMO of **DPS-PXZ** increased, while that of **DPS-PTZ** decreased with rising solvent polarity. Figure 2b illustrates structural comparisons of S_0 conformations in TOL, THF, and DMSO solvents. In the case of **SF2C** and **DPS-PXZ**, their structures remained largely unchanged in these solvents due to the planar and rigid conformation of the **PXZ** group. Conversely, the bonding structure of **PTZ** exhibited significant alterations with varying solvent polarities, particularly in **SFPC**.

Based on the above discussions, the S_0 geometry of the molecules showed minimal alteration with increasing solvent polarity, indicating a subtle change in the frontier molecular orbitals in different solvents. Figures 2c and S2 illustrate the HOMO and LUMO distributions. Observing the HOMO and LUMO distributions in TOL, THF, and DMSO solvents, a remarkable similarity is found for each molecule. In the case of **SF2C**, **SFPC**, and **DPS-PXZ**, their HOMO predominantly extends over the electron-donating groups (**PXZ** and **PTZ**), while the LUMO is primarily localized on the diphenylsulfone acceptor. This conformation indicates a notable separation

https://doi.org/10.1021/acsomega.4c01565
ACS Omega 2024, 9, 26112−26120

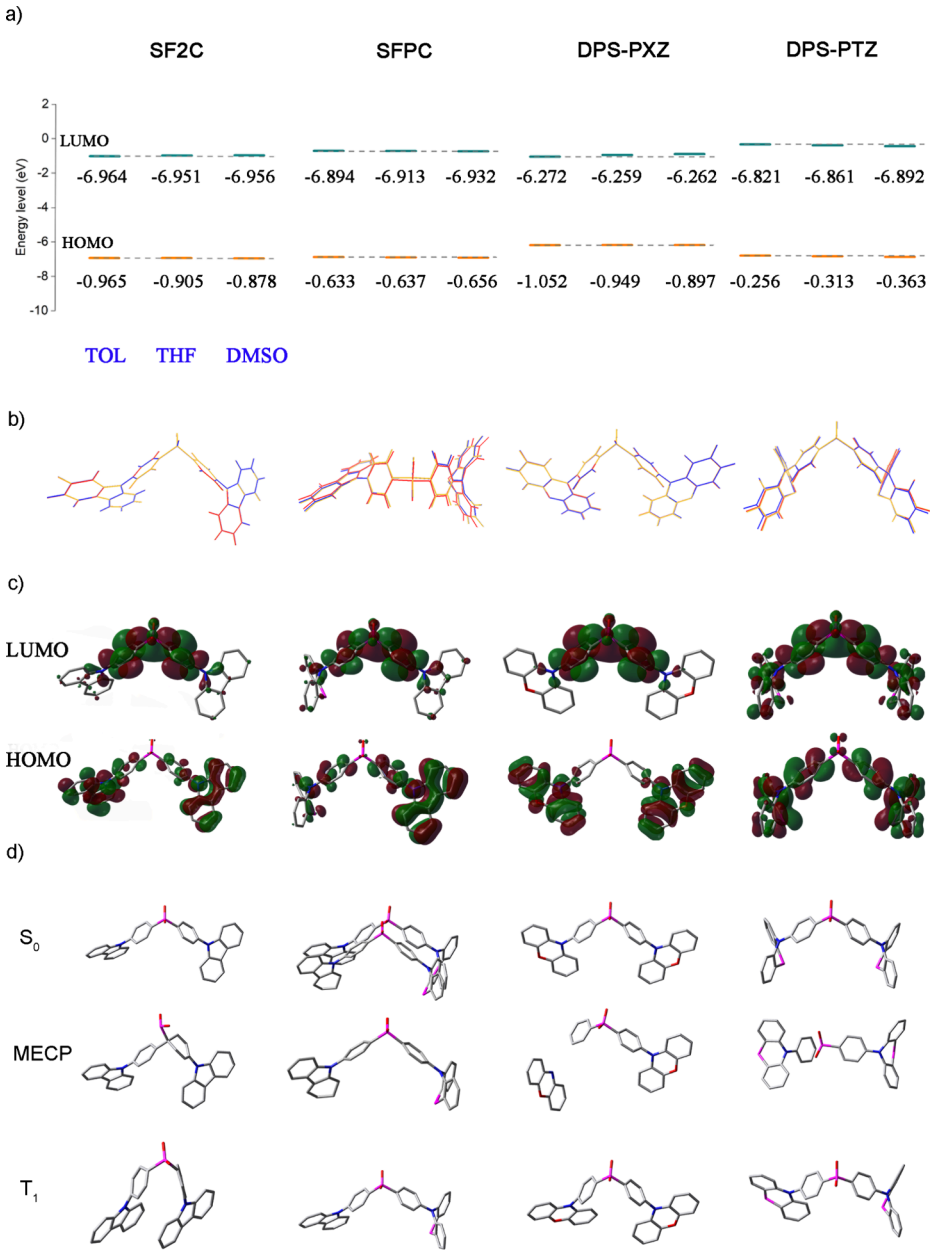

Figure 2. (a) Calculated frontier molecular orbital distributions and energy levels of **SF2C**, **SFPC**, **DPS-PXZ**, and **DPS-PTZ** in toluene/TOL, tetrahydrofuran/THF, and dimethyl sulfoxide/DMSO solvents. (b) Ground-state structures' comparison of **SF2C**, **SFPC**, **DPS-PXZ**, and **DPS-PTZ** in TOL (orange), THF (blue), and DMSO (red) solvents. (c) Frontier molecular orbital distributions of **SF2C**, **SFPC**, **DPS-PXZ**, and **DPS-PTZ** in the TOL solvent. (d) The optimized ground-state, minimum-energy crossing points and triplet excited-state geometries of **SF2C**, **SFPC**, **DPS-PXZ**, and **DPS-PTZ** in the TOL solvent.

between HOMO and LUMO, contributing to improved electronic characteristics. Conversely, for **DPS-PTZ**, the HOMO and LUMO distributions exhibit substantial delocalization across the entire molecular structure, leading to significant overlap between the HOMO and LUMO orbitals. This characteristic indicates less separation between these orbitals compared to the other molecules mentioned, impacting its electronic properties differently.

The structural comparisons among S_0, triplet excited state (T_1), and minimum energy crossing points (MECP) in TOL solvent are depicted in Figure 2d, and those in THF and DMSO solvents are shown in Figure S3. Taking the structures in TOL as an example, for **DPS-PXZ**, the donor and acceptor moieties exhibited near-perpendicular alignment, as evident from the geometric arrangement in Figure 2d. However, for **SF2C**, **SFPC**, **DPS-PXZ**, and **DPS-PTZ**, achieving a MECP structure was unfeasible. For instance, in the case of **DPS-PXZ**, the **PXZ** group in the MECP structure appeared to dissociate partially, while for **DPS-PTZ**, the benzene moiety of diphenylsulfone in the MECP structure was disrupted. These observations highlight the impracticality of attaining a viable MECP structure for these molecules. This failure is advantageous as it ensures the population of the T_1 and facilitates the process of reverse intersystem crossing from T_1 to singlet excited state (S_1) for **SF2C**, **SFPC**, **DPS-PXZ**, and **DPS-PTZ**, leading to the TADF property. Figure S4 depicts the S_0, S_1, and T_1 excited-state potential energy surfaces. If the MECP of S_0 and T_1 is available, more populated T_1 will turn back to the S_0

https://doi.org/10.1021/acsomega.4c01565
ACS Omega 2024, 9, 26112−26120

via nonradiative path. The decreased T_1 population would weaken the conversion between S_1 and T_1 when the S_1-T_1 energy gap is fixed because the conversion between S_1 and T_1 is reversible. Instead, if the MECP of S_0 and T_1 is unavailable, the T_1 population would be in favor of the conversion from S_1 to T_1 through the reverse intersystem crossing process.

The study listed in Table 1 concentrated on assessing singlet−triplet energy splitting (ΔE_{ST}) and spin−orbit coupling (SOC) parameters. The calculated results underscore the importance of a small ΔE_{ST} for facilitating the TADF emission. Notably, the ΔE_{ST} values appear to correlate with the type of solvent used. For instance, the ΔE_{ST} values of **SF2C** and **DPS-PXZ** show an increase with a rise in solvent polarity. Conversely, for **SFPC** and **DPS-PTZ**, the ΔE_{ST} values decrease as the solvent polarity increases. In contrast, the type of solvent seems to exert negligible influence on the SOC values. For instance, the SOC values of **SFPC** are measured at 2.191, 0.306, and 0.293 cm^{-1} in TOL, THF, and DMSO solvents, respectively. Interestingly, the SOC values of **DPS-PTZ** are observed to be close to zero in each solvent.

Table 1. Calculated Singlet−Triplet Energy Splitting and Spin−Orbit Coupling of SF2C, SFPC, DPS-PXZ, and DPS-PTZ in TOL, THF, and DMSO Solvents.

ΔE_{ST}/eV	SF2C	SFPC	DPS-PXZ	DPS-PTZ
TOL	0.289	0.536	0.247	0.335
THF	0.367	0.496	0.464	0.334
DMSO	0.536	0.471	0.578	0.333
SOC/cm^{-1}	**SF2C**	**SFPC**	**DPS-PXZ**	**DPS-PTZ**
TOL	0.226	0.291	0.824	0.028
THF	0.226	0.306	0.816	0.000
DMSO	0.142	0.293	0.846	0.014

These molecules share a common diphenylsulfone acceptor but possess distinct donor groups, namely, **Cz**, **PXZ**, and **PTZ**. Remarkably, a disparity in their properties arises from the alteration of just one donor unit. To delve deeper into the mechanisms behind these intriguing AIE phenomena, this study includes molecular dynamics investigations conducted on both single molecules and their aggregate states. These studied molecules are in donor−acceptor models, and it is observed that the variation in geometry following electron excitation can often be attributed to the dihedral angle between the donor and acceptor units. For example, the atomistic molecular dynamics simulation of deposition process, based on fluorescent molecules, discovered that the torsion angles between donor and acceptor groups have a broadened distribution around 90° due to the thermal fluctuation and intermolecular interaction.[46] Based on well-known 1,2-bis-(carbazol-9-yl)-4,5 dicyanobenzene (2CzPN) and (4CzIPN), the theoretical simulation of bulk amorphous phase also indicated that the torsion angles between donor and acceptor are in a broad distribution, and the reverse intersystem crossing is a dynamical process with the varying molecular structures.[47,48] Consequently, the changes in this angle between the donor and acceptor units can significantly influence the molecular behavior, contributing to the observed differences in properties among molecules with different donor groups.

Therefore, this work was focused on analyzing the changes in DA1 and DA2 dihedral angles (in Figure 3a). The DA1 and DA2 concerning single molecule and clusters comprising 300 molecules at temperatures of 298 and 500 K, as depicted in Figure 3b. For **SF2C** and **DPS-PXZ**, whether in their single molecule or aggregate state, minimal changes in DA1 and DA2 are observed, regardless of the temperature (298 or 500 K). Similar stability was found for DA1 of **SFPC**. However, the DA2 of **SFPC** in the single molecule exhibited significant variation with a temperature shift from 298 to 500 K. Interestingly, while the DA2 of **SFPC** in the single molecule was strongly influenced by temperature, its counterpart in the aggregate state experienced relatively minor alterations. This suggests that the surrounding molecules in the **SFPC** cluster tend to constrain the rotation of DA2, consequently avoiding nonradiative decay channels. The DA1 and DA2 cases for **DPS-PTZ** are interesting; at 298 K, the DA1 in the single molecule exhibited minor fluctuations. However, at 500 K, the DA1 showed a substantial decrease initially from 0 to 100 ps, followed by stabilization from 100 to 200 ps. Conversely, the DA1 of **DPS-PTZ** in the aggregate state remained relatively stable at both 298 and 500 K, indicating that changes in temperature had minimal impact on the dihedral angle between the donor and acceptor groups in the aggregate state. Moreover, at 500 K, the DA2 of **DPS-PTZ** in the aggregate state demonstrated significant changes. These findings suggest that temperature and the surrounding environment exert less influence on **Cz** and **PXZ** compared to **PTZ**. **Cz** and **PXZ** with their planar and rigid conformations appear to be less affected by the temperature and environmental changes. However, the bonding **PTZ** group exhibits a more considerable sensitivity to temperature variations and environmental conditions, leading to noticeable fluctuations in both DA1 and DA2.

Molecular dynamics simulations focused on analyzing the variations of DA1 and DA2 dihedral angles in a TOL solvent environment (in Figure 3c). The boxes comprising 200 solvents with five or 35 target molecules are delineated. The calculated results revealed notable differences in DA1 and DA2 between the boxes housing 35 target molecules versus those with only five. In particular, for **DPS-PTZ**, the boxes with 35 molecules displayed significantly reduced fluctuations in DA1, approaching a more stable horizontal trend during certain time periods. This illustrates that the dihedral angle between the donor and acceptor becomes less fluctuant with an increase in the number of surrounding target molecules. This sensitivity to the surrounding environment indicates that higher target molecule densities result in less variation in these dihedral angles. In polar solvents, the rotatable D−A bond tends to exhibit greater flexibility. However, in an aggregate state or low-polarity environments, this flexibility is restrained due to the less polar nature of the local environment, thereby restricting the twist of the D−A bond. This observation aligns with studies suggesting that doping in thin films mirrors behavior akin to low-polarity solvent environments. Taking the box containing 200 solvents and 35 target molecules as an example, it was observed that **SF2C** and **SFPC** in TOL solvent exhibited significant fluctuations in DA1 and DA2. Conversely, **DPS-PTZ** showed minimal fluctuations in low-polarity solvent conditions, suggesting that the twist in **PTZ** is constrained. Molecular dynamics investigations further indicate that in thin film the **PTZ** component of **DPS-PTZ** experiences restricted twisting, contributing to its AIE property.

The AIE characteristic is widely acknowledged to arise from a restricted rotation in the aggregate state. To further explore this, a comparison between S_0 and S_1 geometries in different solvents was conducted, utilizing root mean square deviation

https://doi.org/10.1021/acsomega.4c01565
ACS Omega 2024, 9, 26112−26120

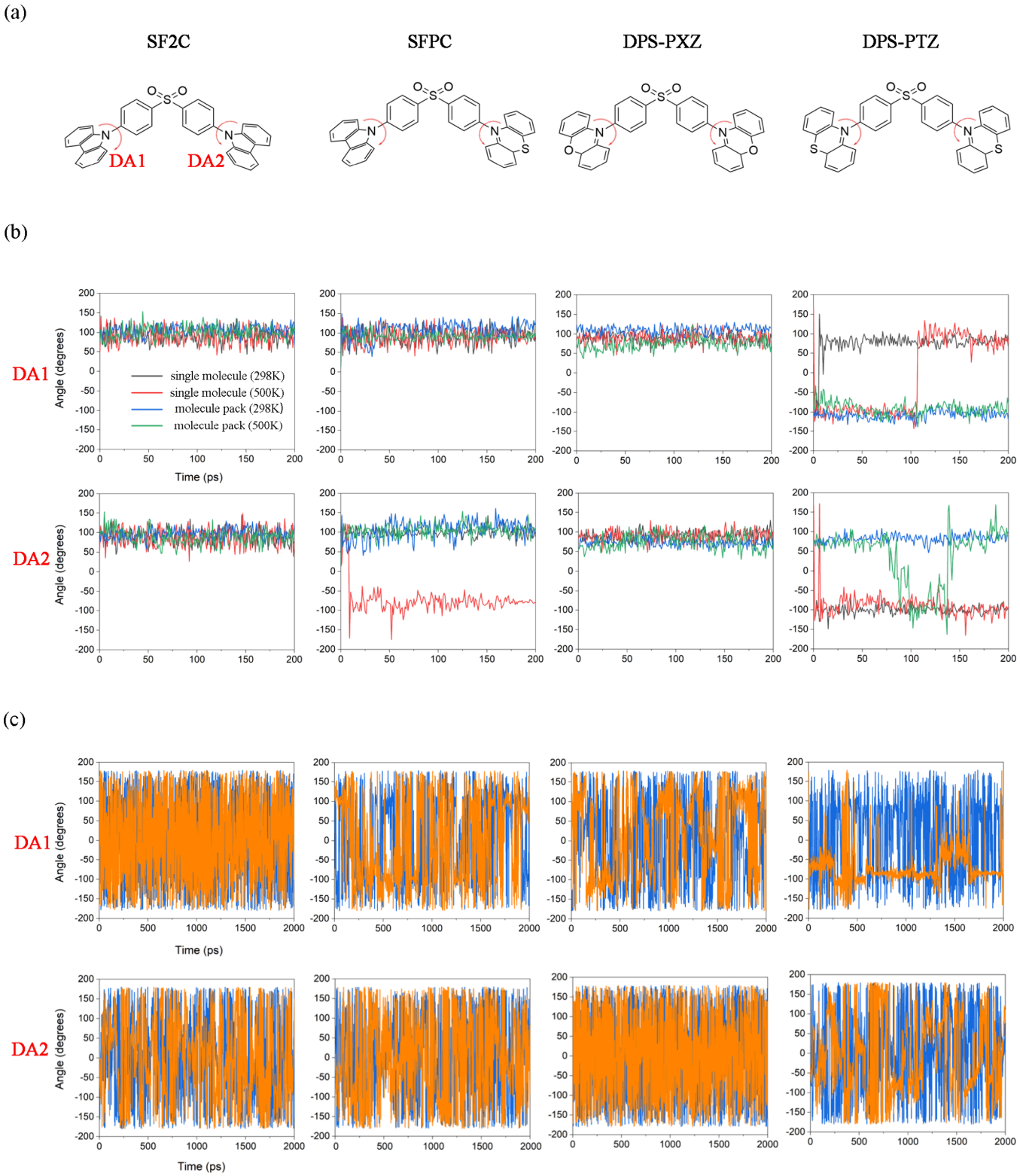

Figure 3. (a) Molecular structures of **SF2C**, **SFPC**, **DPX-PXZ**, and **DPS-PTZ**. (b) Plots of DA1 and DA2 angles for single molecule and 300 molecular cluster as a function of time. (c) Plots of DA1 and DA2 angles for boxes containing 200 solvents and 5 (in blue) or 35 (in yellow) target molecules as a function of time.

(RMSD) parameter. Smaller RMSD values indicate minimal structural changes during the relaxation process of the electron in the excited state. Figure 4a illustrates that **DPS-PTZ** exhibits relatively larger RMSD values in comparison to **SF2C**, **SFPC**, and **DPS-PXZ**. This suggests more significant structural alterations during the excited state relaxation process in **DPS-PTZ**. In particular, the geometric comparison highlights a noticeable increase in the twist of the **PTZ** component within **DPS-PTZ**. This substantial twist indicates a higher tendency for nonradiative decay in **DPS-PTZ**. However, molecular

https://doi.org/10.1021/acsomega.4c01565
ACS Omega 2024, 9, 26112−26120

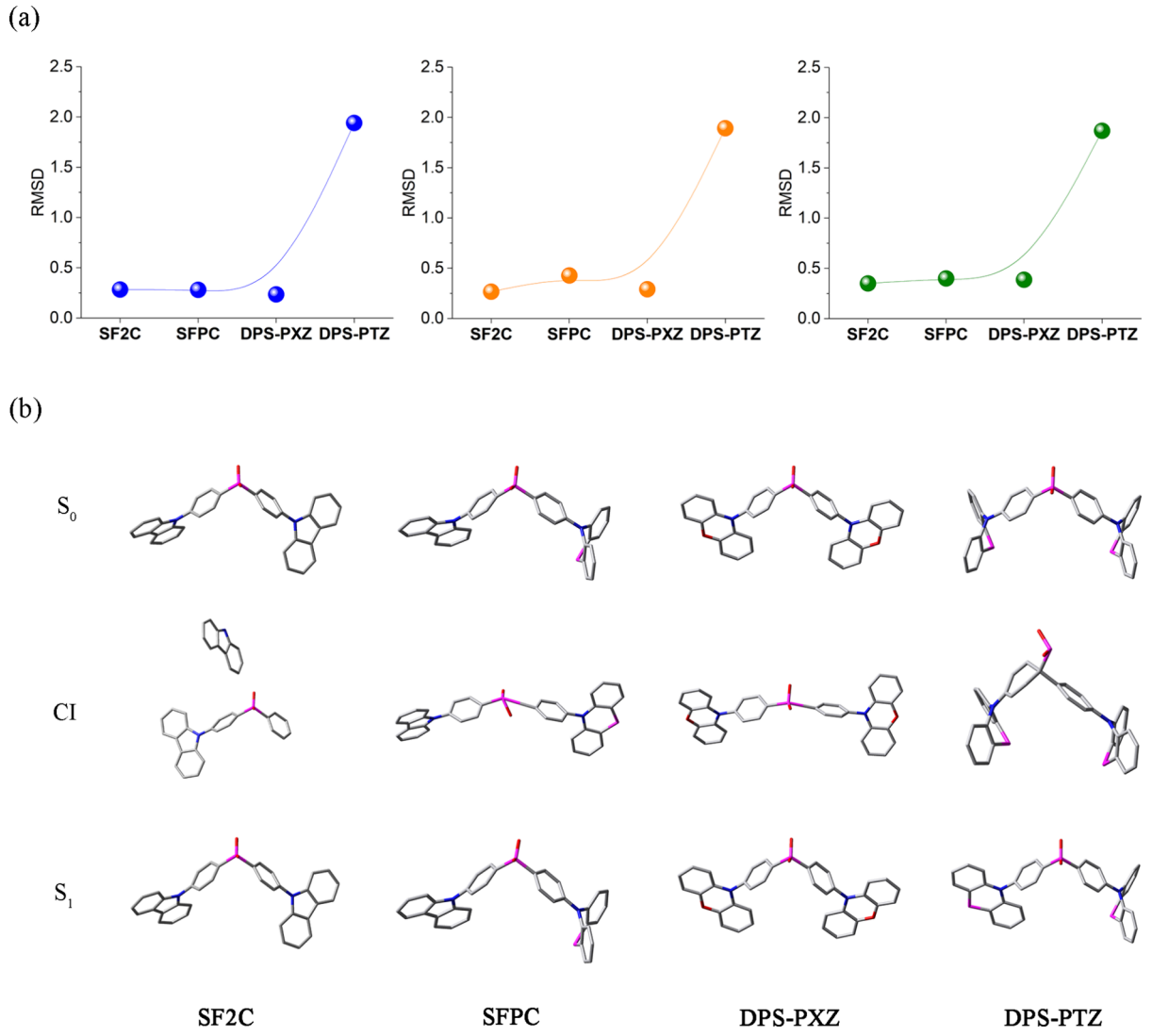

Figure 4. (a) Root-mean-square deviation between the ground-state and singlet excited-state geometries of **SF2C**, **SFPC**, **DPS-PXZ**, and **DPS-PTZ** in TOL. (b) Optimized ground-state, conical interaction, and singlet excited-state geometries of **SF2C**, **SFPC**, **DPS-PXZ**, and **DPS-PTZ** in TOL.

dynamics results indicate that this decay is remarkably suppressed in the aggregate environment. In addition, we have performed S_1 potential energy surface by twisting **Cz**, **PXZ**, and **PTZ** groups with a range from 0 to 90° with a scan step of 10° (Figure S5). Different from **Cz** group, the oscillator strength values undergo a small variation with twisting **PXZ** or **PTZ** group, indicating that the AIE behaviors of **DPS-PXZ** and **DPS-PTZ** possibly originated from the part of nonradiative decay. The combination of molecular dynamics investigations and quantum calculations strongly suggests that the AIE property observed in **DPS-PTZ** originates from the restriction imposed on the **PTZ** component in the aggregate state. This restriction in the aggregate state acts as a critical factor in inhibiting the nonradiative decay of **DPS-PTZ**, consequently leading to its AIE behavior.

The further optimization of the S_0/S_1 conical intersection (CI) structures of **SF2C**, **SFPC**, **DPS-PXZ**, and **DPS-PTZ** in TOL using the ORCA program was conducted and is depicted in Figure 4b. Upon analysis, it was observed that the S_0 and S_1 structures of **SF2C**, **SFPC**, and **DPS-PXZ** are notably similar, confirmed by their small RMSD values (in Figure 4a). However, for **SF2C**, the **Cz** component displays dissociation in the CI structure, rendering it an unreasonable conformation. In the CI structure of **SFPC**, the previously bonding **PTZ** component adopts a planar conformation. This transition from bonding to a planar structure is distinctive in the CI conformation of **SFPC**. Similarly, for **DPS-PXZ**, the structures of CI, S_0, and S_1 are highly similar, displaying nearly vertical donor and acceptor groups. The primary difference lies in the C−S−C angle, which is greater in the CI structure compared with S_0 and S_1 structures. Consequently, the CI structure of **DPS-PXZ** easily transitions via twisting C−S−C angle in a loose solvent environment to reach S_0 through a nonradiative pathway. However, in an aggregate state, the suppression of C−S−C twisting makes it difficult to achieve a CI structure. That explains why the S_1 state emits fluorescence and elucidates the underlying reason for the AIE property observed in **DPS-PXZ**. On the other hand, **DPS-PTZ** showcases significant discrepancies between S_0 and S_1, and the **PTZ** group in the S_1 structure even adopts a planar conformation, resulting in an unattainable CI structure. As a result, achieving the CI structure for **DPS-PTZ** is rendered impossible due to these structural variations between the S_0 and S_1 conformations.

https://doi.org/10.1021/acsomega.4c01565
ACS Omega 2024, 9, 26112−26120

3. CONCLUSIONS

The aim of this study was to uncover the underlying AIE and TADF mechanisms involving phenoxazine (**PXZ**) and phenothiazine (**PTZ**) groups. The TADF property of four molecules was established through small singlet−triplet energy splitting (ΔE_{ST}) and substantial spin−orbit coupling (SOC) constants. Notably, the absence of a minimum energy crossing point (MECP) structure was instrumental in ensuring the population of the triplet state (T_1) and facilitating reverse intersystem crossing (RISC) from T_1 to the singlet state (S_1) for all molecules. The ground-state (S_0) structures of **SF2C** and **DPS-PXZ** remained relatively unaffected by varying TOL, THF, and DMSO solvents due to the planar and rigid conformations of the **PXZ** group. However, **SFPC** experienced considerable structural changes attributed to the bonding structure of the **PTZ** group, resulting in variations in solvent polarity. Moreover, while the RMSD values between S_0 and S_1 were minimal for **SF2C**, **SFPC**, and **DPS-PXZ**, **DPS-PTZ** exhibited comparatively larger RMSD values, indicating a noticeable increase in the **PTZ** twist. This higher tendency for nonradiative decay in **DPS-PTZ** was found to be substantially suppressed in an aggregate environment, leading to its AIE behavior. The integration of molecular dynamics studies and quantum calculations highlighted that the AIE property observed in **DPS-PTZ** stemmed from the restricted behavior of the **PTZ** group in the aggregate state. In thin films, the surrounding environment constrained the **PTZ** twist, reducing nonradiative decay and prompting the AIE property of **DPS-PTZ**. Furthermore, the density functional results underscored that in loose solvent environments, the CI structure of **DPS-PXZ** was easily attainable via the C−S−C twist, transitioning to S_0 through a nonradiative pathway. However, in an aggregate state, the suppression of the C−S−C twist made achieving the CI structure challenging, with the fluorescence-emitting S_1 state becoming prominent. The formation of the CI structure in **DPS-PXZ** emerged as a pivotal factor contributing to its AIE property. Due to different AIE mechanisms, the further modifications of **DPS-PXZ** and **DPS-PTZ** are different. To enhance luminescence efficiency, restricting the rotation of the donor−acceptor bond is effective for **DPS-PTZ**, whereas suppressing the C−S−C twist to prevent the formation of the CI structure is effective for **DPS-PXZ**. Consequently, understanding these mechanisms holds significant promise in offering design guidelines for developing new AIE systems with practical applications.

■ ASSOCIATED CONTENT

Supporting Information

The Supporting Information is available free of charge at https://pubs.acs.org/doi/10.1021/acsomega.4c01565.

Optimized structures of DPS-PTZ; frontier molecular orbital distributions of SF2C; optimized ground state, minimum energy crossing points; ground-state (S0), singlet (S1), and triplet; and oscillator strength changes with varying dihedral angles (PDF)

■ AUTHOR INFORMATION

Corresponding Authors

Ying Gao − *Jilin Provincial Key Laboratory of Straw−Based Functional Materials, Institute for Interdisciplinary Biomass Functional Materials Studies, Jilin Engineering Normal University, Changchun 130052, China;* orcid.org/0000-0002-3083-8555; Email: gaoy029@163.com

Xiao-Dong Yang − *Jilin Provincial Key Laboratory of Straw−Based Functional Materials, Institute for Interdisciplinary Biomass Functional Materials Studies, Jilin Engineering Normal University, Changchun 130052, China;* Email: y86908051@126.com

Authors

Yan-Ping Lin − *Key Laboratory of Bionic Engineering (Ministry of Education), Jilin University, Changchun 130022, P. R. China; Jilin Provincial Key Laboratory of Straw−Based Functional Materials, Institute for Interdisciplinary Biomass Functional Materials Studies, Jilin Engineering Normal University, Changchun 130052, China*

Yong Wu − *Faculty of Chemistry, Northeast Normal University, Changchun, Jilin 130024, China;* orcid.org/0000-0002-6806-1817

Complete contact information is available at: https://pubs.acs.org/10.1021/acsomega.4c01565

Notes

The authors declare no competing financial interest.

■ ACKNOWLEDGMENTS

The authors gratefully acknowledge financial support from the National Natural Science Foundation of China (51902124), Department Science and Technology of Jilin Province (20210203131SF), Department of Education of Jilin Province, and Technology Research Projects (JJKH20230223KJ). The computational details are listed in Supporting Information.

■ REFERENCES

(1) Tang, C. W.; VanSlyke, S. A. Organic electroluminescent diodes. *Appl. Phys. Lett.* **1987**, *51*, 913−915.

(2) Uoyama, H.; Goushi, K.; Shizu, K.; Nomura, H.; Adachi, C. Highly efficient organic light-emitting diodes from delayed fluorescence. *Nature* **2012**, *492*, 234−238.

(3) Zhang, Q.; Li, B.; Huang, S.; Nomura, H.; Tanaka, H.; Adachi, C. Efficient blue organic light-emitting diodes employing thermally activated delayed fluorescence. *Nat. Photonics* **2014**, *8*, 326−332.

(4) Kaji, H.; Suzuki, H.; Fukushima, T.; Shizu, K.; Suzuki, K.; Kubo, S.; Komino, T.; Oiwa, H.; Suzuki, F.; Wakamiya, A.; Murata, Y.; Adachi, C. Purely organic electroluminescent material realizing 100% conversion from electricity to light. *Nat. Commun.* **2015**, *6*, 8476.

(5) Dias, F. B.; Bourdakos, K. N.; Jankus, V.; Moss, K. C.; Kamtekar, K. T.; Bhalla, V.; Santos, J.; Bryce, M. R.; Monkman, A. P. Triplet Harvesting with 100% Efficiency by Way of Thermally Activated Delayed Fluorescence in Charge Transfer OLED Emitters. *Adv. Mater.* **2013**, *25*, 3707−3714.

(6) Chen, Y.; Lam, J. W. Y.; Kwok, R. T. K.; Liu, B.; Tang, B. Z. Aggregation-induced emission: fundamental understanding and future developments. *Mater. Horiz.* **2019**, *6*, 428−433.

(7) Méhes, G.; Nomura, H.; Zhang, Q.; Nakagawa, T.; Adachi, C. Enhanced Electroluminescence Efficiency in a Spiro-Acridine Derivative through Thermally Activated Delayed Fluorescence. *Angew. Chem., Int. Ed.* **2012**, *51*, 11311−11315.

(8) Luo, J.; Xie, Z.; Lam, J. W. Y.; Cheng, L.; Chen, H.; Qiu, C.; Kwok, H. S.; Zhan, X.; Liu, Y.; Zhu, D.; Tang, B. Z. Aggregation-induced emission of 1-methyl-1,2,3,4,5-pentaphenylsilole. *Chem. Commun.* **2001**, 1740−1741.

(9) Hong, Y.; Lam, J. W. Y.; Tang, B. Z. Aggregation-induced emission: phenomenon, mechanism and applications. *Chem. Commun.* **2009**, 4332−4353.

(10) Zhao, Z.; Zhang, H.; Lam, J. W. Y.; Tang, B. Z. Aggregation-Induced Emission: New Vistas at the Aggregate Level. *Angew. Chem., Int. Ed.* **2020**, *59*, 9888−9907.
(11) Mei, J.; Leung, N. L. C.; Kwok, R. T. K.; Lam, J. W. Y.; Tang, B. Z. Aggregation-Induced Emission: Together We Shine, United We Soar! *Chem. Rev.* **2015**, *115*, 11718−11940.
(12) Han, T.; Yan, D.; Wu, Q.; Song, N.; Zhang, H.; Wang, D. Aggregation-Induced Emission: A Rising Star in Chemistry and Materials Science. *Chin. J. Chem.* **2021**, *39*, 677−689.
(13) Würthner, F. Aggregation-Induced Emission (AIE): A Historical Perspective. *Angew. Chem.* **2020**, *59*, 14192−14196.
(14) Peng, Q.; Yi, Y.; Shuai, Z.; Shao, J. Toward Quantitative Prediction of Molecular Fluorescence Quantum Efficiency: Role of Duschinsky Rotation. *J. Am. Chem. Soc.* **2007**, *129*, 9333−9339.
(15) Zhao, Z.; Lu, P.; Lam, J. W. Y.; Wang, Z.; Chan, C. Y. K.; Sung, H. H. Y.; Williams, I. D.; Ma, Y.; Tang, B. Z. Molecular anchors in the solid state: Restriction of intramolecular rotation boosts emission efficiency of luminogen aggregates to unity. *Chem. Sci.* **2011**, *2*, 672−675.
(16) Yang, Z.; Qin, W.; Leung, N. L. C.; Arseneault, M.; Lam, J. W. Y.; Liang, G.; Sung, H. H. Y.; Williams, I. D.; Tang, B. Z. A mechanistic study of AIE processes of TPE luminogens: intramolecular rotation vs. configurational isomerization. *J. Mater. Chem. C* **2016**, *4*, 99−107.
(17) Leung, N. L. C.; Xie, N.; Yuan, W.; Liu, Y.; Wu, Q.; Peng, Q.; Miao, Q.; Lam, J. W. Y.; Tang, B. Z. Restriction of Intramolecular Motions: The General Mechanism behind Aggregation-Induced Emission. *Chem.—Eur. J.* **2014**, *20*, 15349−15353.
(18) Ren, Y.; Lam, J. W. Y.; Dong, Y.; Tang, B. Z.; Wong, K. S. Enhanced Emission Efficiency and Excited State Lifetime Due to Restricted Intramolecular Motion in Silole Aggregates. *J. Phys. Chem. B* **2005**, *109*, 1135−1140.
(19) Ding, W.-L.; Peng, X.-L.; Cui, G.-L.; Li, Z.-S.; Blancafort, L.; Li, Q.-S. Potential-Energy Surface and Dynamics Simulation of THBDBA: An Annulated Tetraphenylethene Derivative Combining Aggregation-Induced Emission and Switch Behavior. *ChemPhotoChem.* **2019**, *3*, 814−824.
(20) An, B.-K.; Gierschner, J.; Park, S. Y. π-Conjugated Cyanostilbene Derivatives: A Unique Self-Assembly Motif for Molecular Nanostructures with Enhanced Emission and Transport. *Acc. Chem. Res.* **2012**, *45*, 544−554.
(21) Naito, H.; Nishino, K.; Morisaki, Y.; Tanaka, K.; Chujo, Y. Solid-State Emission of the Anthracene-o-Carborane Dyad from the Twisted-Intramolecular Charge Transfer in the Crystalline State. *Angew. Chem., Int. Ed.* **2017**, *56*, 254−259.
(22) Qian, Y.; Cai, M.-M.; Xie, L.-H.; Yang, G.-Q.; Wu, S.-K.; Huang, W. Restriction of Photoinduced Twisted Intramolecular Charge Transfer. *ChemPhysChem* **2011**, *12*, 397−404.
(23) Hu, R.; Li, S.; Zeng, Y.; Chen, J.; Wang, S.; Li, Y.; Yang, G. Understanding the aggregation induced emission enhancement for a compound with excited state intramolecular proton transfer character. *Phys. Chem. Chem. Phys.* **2011**, *13*, 2044−2051.
(24) Chen, M.; Li, L.; Nie, H.; Tong, J.; Yan, L.; Xu, B.; Sun, J. Z.; Tian, W.; Zhao, Z.; Qin, A.; Tang, B. Z. Tetraphenylpyrazine-based AIEgens: facile preparation and tunable light emission. *Chem. Sci.* **2015**, *6*, 1932−1937.
(25) Zhao, Z.; He, B.; Tang, B. Z. Aggregation-induced emission of siloles. *Chem. Sci.* **2015**, *6*, 5347−5365.
(26) Li, Y.; Shao, A.; Wang, Y.; Mei, J.; Niu, D.; Gu, J.; Shi, P.; Zhu, W.; Tian, H.; Shi, J. Morphology-Tailoring of a Red AIEgen from Microsized Rods to Nanospheres for Tumor-Targeted Bioimaging. *Adv. Mater.* **2016**, *28*, 3187−3193.
(27) Yu, C. Y. Y.; Xu, H.; Ji, S.; Kwok, R. T. K.; Lam, J. W. Y.; Li, X.; Krishnan, S.; Ding, D.; Tang, B. Z. Mitochondrion-Anchoring Photosensitizer with Aggregation-Induced Emission Characteristics Synergistically Boosts the Radiosensitivity of Cancer Cells to Ionizing Radiation. *Adv. Mater.* **2017**, *29*, No. 1606167.
(28) Zhang, J.; Ma, S.; Fang, H.; Xu, B.; Sun, H.; Chan, I.; Tian, W. Insights into the origin of aggregation enhanced emission of 9,10-distyrylanthracene derivatives. *Mater. Chem. Front.* **2017**, *1*, 1422−1429.
(29) Zhang, J.; Zhang, H.; Lam, J. W. Y.; Tang, B. Z. Restriction of Intramolecular Motion(RIM): Investigating AIE Mechanism from Experimental and Theoretical Studies. *Chem. Res. Chinese U.* **2021**, *37*, 1−15.
(30) Chen, J.; Law, C. C. W.; Lam, J. W. Y.; Dong, Y.; Lo, S. M. F.; Williams, I. D.; Zhu, D.; Tang, B. Z. Synthesis, Light Emission, Nanoaggregation, and Restricted Intramolecular Rotation of 1,1-Substituted 2,3,4,5-Tetraphenylsiloles. *Chem. Mater.* **2003**, *15*, 1535−1546.
(31) Shustova, N. B.; McCarthy, B. D.; Dincă, M. Turn-On Fluorescence in Tetraphenylethylene-Based Metal−Organic Frameworks: An Alternative to Aggregation-Induced Emission. *J. Am. Chem. Soc.* **2011**, *133*, 20126−20129.
(32) Yu, Q.; Zhang, J.; Lam, J. W. Y.; Yang, D.; Sun, J.; Tang, B. Z. Tunable Room Temperature Phosphorescence in Heavy-Atom-Free Metal−Organic Frameworks by Ligand Functionalization. *ACS Mater. Lett.* **2023**, *5*, 2691−2699.
(33) Zou, H.; Liu, L.; Zhang, S.; Miao, X.; Ying, L.; Deng, W.; Cao, Y. Different Stepwise Growth Mechanism of AIE-Active Tetraphenylethylene-Functionalized Metal−Organic Frameworks on Au(111) and Cu(111) Surfaces. *J. Phys. Chem. Lett.* **2023**, *14*, 489−498.
(34) He, B.; Ye, S.; Guo, Y.; Chen, B.; Xu, X.; Qiu, H.; Zhao, Z. Aggregation-enhanced emission and efficient electroluminescence of conjugated polymers containing tetraphenylethene units. *Sci. China Chem.* **2013**, *56*, 1221−1227.
(35) Gao, B.-R.; Wang, H.-Y.; Hao, Y.-W.; Fu, L.-M.; Fang, H.-H.; Jiang, Y.; Wang, L.; Chen, Q.-D.; Xia, H.; Pan, L.-Y.; Ma, Y.-G.; Sun, H.-B. Time-Resolved Fluorescence Study of Aggregation-Induced Emission Enhancement by Restriction of Intramolecular Charge Transfer State. *J. Phys. Chem. B* **2010**, *114*, 128−134.
(36) Hu, R.; Lager, E.; Aguilar-Aguilar, A.; Liu, J.; Lam, J. W. Y.; Sung, H. H. Y.; Williams, I. D.; Zhong, Y.; Wong, K. S.; Peña-Cabrera, E.; Tang, B. Z. Twisted Intramolecular Charge Transfer and Aggregation-Induced Emission of BODIPY Derivatives. *J. Phys. Chem. C* **2009**, *113*, 15845−15853.
(37) Guo, J.; Li, X.; Nie, H.; Luo, W.; Gan, S.; Hu, S.; Hu, R.; Qin, A.; Zhao, Z.; Su, S.; Tang, B. Z. Achieving High-Performance Nondoped OLEDs with Extremely Small Efficiency Roll-Off by Combining Aggregation-Induced Emission and Thermally Activated Delayed Fluorescence. *Adv. Funct. Mater.* **2017**, *27*, No. 1606458.
(38) Liu, J.; Zhang, H.; Hu, L.; Wang, J.; Lam, J. W. Y.; Blancafort, L.; Tang, B. Z. Through-Space Interaction of Tetraphenylethylene: What, Where, and How. *J. Am. Chem. Soc.* **2022**, *144*, 7901−7910.
(39) Xu, S.; Liu, T.; Mu, Y.; Wang, Y.-F.; Chi, Z.; Lo, C.-C.; Liu, S.; Zhang, Y.; Lien, A.; Xu, J. An Organic Molecule with Asymmetric Structure Exhibiting Aggregation-Induced Emission, Delayed Fluorescence, and Mechanoluminescence. *Angew. Chem., Int. Ed.* **2015**, *54*, 874−878.
(40) Xie, Z.; Chen, C.; Xu, S.; Li, J.; Zhang, Y.; Liu, S.; Xu, J.; Chi, Z. White-Light Emission Strategy of a Single Organic Compound with Aggregation-Induced Emission and Delayed Fluorescence Properties. *Angew. Chem.* **2015**, *54*, 7181−7184.
(41) Gan, S.; Luo, W.; He, B.; Chen, L.; Nie, H.; Hu, R.; Qin, A.; Zhao, Z.; Tang, B. Z. Integration of aggregation-induced emission and delayed fluorescence into electronic donor−acceptor conjugates. *J. Mater. Chem. C* **2016**, *4*, 3705−3708.
(42) Lee, I. H.; Song, W.; Lee, J. Y. Aggregation-induced emission type thermally activated delayed fluorescent materials for high efficiency in non-doped organic light-emitting diodes. *Org. Electron.* **2016**, *29*, 22−26.
(43) Wu, H.; Fan, X.; Wang, H.; Huang, F.; Xiong, X.; Shi, Y.; Wang, K.; Yu, J.; Zhang, X. Conformational isomerization: A novel mechanism to realize the AIE-TADF behaviors. *Aggregate* **2023**, *4*, No. e243.
(44) Wu, X.; Gong, C.; Jiang, X.; Gao, J.; Li, M.; He, R.; Chen, P.; Shen, W. Face-to-face order-packed mode promotes thermally

https://doi.org/10.1021/acsomega.4c01565
ACS Omega 2024, 9, 26112−26120

activated delayed fluorescence to achieve stronger aggregation-induced emission. *J. Sci.: Adv. Mater. Dev.* **2022**, *7*, No. 100432.
(45) Aydemir, M.; Xu, S.; Chen, C.; Bryce, M. R.; Chi, Z.; Monkman, A. P. Photophysics of an Asymmetric Donor−Acceptor−Donor′ TADF Molecule and Reinterpretation of Aggregation-Induced TADF Emission in These Materials. *J. Phys. Chem. C* **2017**, *121*, 17764−17772.
(46) Hu, T.-P.; Han, G.-C.; Tu, Z.-Y.; Duan, R.-H.; Yi, Y.-P. Origin of high efficiencies for thermally activated delayed fluorescence organic light-emitting diodes: Atomistic insight into molecular orientation and torsional disorder. *J. Phys. Chem. C* **2018**, *122*, 27191−27197.
(47) Moral, M.; Son, W.-J.; Sancho-Garcia, J.-C.; Olivier, Y.; Muccioli, L. Cost-effective force field tailored for solid-phase simulations of OLED materials. *J. Chem. Theory Comput.* **2015**, *11*, 3383−3392.
(48) Olivier, Y.; Yurash, B.; Muccioli, L.; D'Avino, G.; Mikhnenko, O.; Sancho-García, J. C.; Adachi, C.; Nguyen, T.-Q.; Beljonne, D. Nature of the singlet and triplet excitations mediating thermally activated delayed fluorescence. *Phys. Rev. Mater.* **2017**, *1*, No. 075602.

https://doi.org/10.1021/acsomega.4c01565
ACS Omega 2024, 9, 26112−26120